Supporting Information

Pyro-Phototronic Effect Enhanced MXene/ZnO Heterojunction Nanogenerator for Light Energy Harvesting

Mingyan Xue [1,2], Fangpei Li [1,2,3,*], Wenbo Peng [1,2,*], Quanzhe Zhu [4] and Yongning He [1,2,*]

[1] School of Microelectronics, Xi'an Jiaotong University, Xi'an 710049, China
[2] The Key Lab of Micro-Nano Electronics and System Integration of Xi'an City, Xi'an 710049, China
[3] State Key Laboratory of Solidification Processing, Key Laboratory of Radiation Detection Materials and Devices, School of Materials Science and Engineering, Northwestern Polytechnical University, Xi'an 710072, China
[4] Shaanxi Advanced Semiconductor Technology Center Co., Ltd, Xi'an 710077, China
* Correspondence: fangpeilee@163.com (F.L.); wpeng33@mail.xjtu.edu.cn (W.P.); yongning@mail.xjtu.edu.cn (Y.H.)

Supplementary Note

Calculation of applied strain

Because one end of the flexible substrate is fixed and the other end is manipulated with a small displacement along the substrate's thickness direction, *i.e.* the *c*-axis of ZnO, therefore, the flexible substrate can be assumed to be bent with a radius of *R*, as illustrated in **Figure S14**. The thickness of the flexible substrate is *D* and the as-fabricated device has a length of *l* and thickness of *d*. Because we have $R >> D$ (7 mil ≈ 177.8 μm) and $D >> d$ (a few microns in maximum), the strain ε of the device approximatively equals to the strain of the flexible substrate, which can be expressed as $\varepsilon = D / (2R)$.

Working mechanism of pyro-phototronic effect in MXene/ZnO heterojunction nanogenerator

Figure 1e presents the working mechanism of the MXene/ZnO heterojunction pyro-phototronic nanogenerator. The detailed general explanation is as below.

From the measured results as shown in **Figure 2a**, the transient current shows a clear four-stages behavior, which directly corresponds to the pyro-phototronic effect. The fundamental mechanism is illustrated in **Figure 1e**.

First, once the incident light is absorbed by the MXene/ZnO heterojunction, the photon energy would produce photo–generated electrons and holes in ZnO, yielding the photovoltaic effect induced current. Simultaneously, the temperature of ZnO would also increase to some degree, yielding a positive transient temperature rise rate $dT/dt > 0$. Considering that ZnO is a pyroelectric semiconductor, this positive dT/dt would produce a transient pyroelectric current spike. The photovoltaic effect induced current combine with the transient pyroelectric current spike, presenting a high current peak, which is clearly the stage–I.

Then, as the light keeps illuminating steadily, the temperature of ZnO surely saturates to a stable value, indicating that $dT/dt = 0$. As a result, the pyroelectric current spike disappears and the current of MXene/ZnO then decreases gradually to a saturation value, which should be induced by the photovoltaic effect (i.e., the stage–II). To better recognize these different current components, the pyroelectric current spike is named as I_{pyro} and the photovoltaic effect induced current is named as I_{photo}. Therefore, the total current at stage–I should be the sum of them, which is named as $I_{pyro+photo} = I_{pyro} + I_{photo}$, indicating the cooperation of pyroelectric and photovoltaic effects, i.e., the pyro-phototronic effect.

The stage–III is the reverse part of stage–I actually. When the illumination turns off, there is no photo-excited carriers generated in the ZnO. As a result, the response current would decrease. At the same time, the temperature of ZnO would of course decrease and this yields a negative transient temperature fall rate $dT/dt < 0$. Consequently, a reverse transient pyroelectric current spike occurs at the stage–III.

Surely, the temperature of ZnO would quickly become stable again and thus the dT/dt goes back to zero again under dark condition, meaning that the total current finally recovers to the dark current (i.e., the stage–IV). These results clearly demonstrate that, the pyro-phototronic effect could significantly enhance the photoresponse of the MXene/ZnO heterojunction and hence the performance of light energy harvesting nanogenerator.

Supplementary Figures

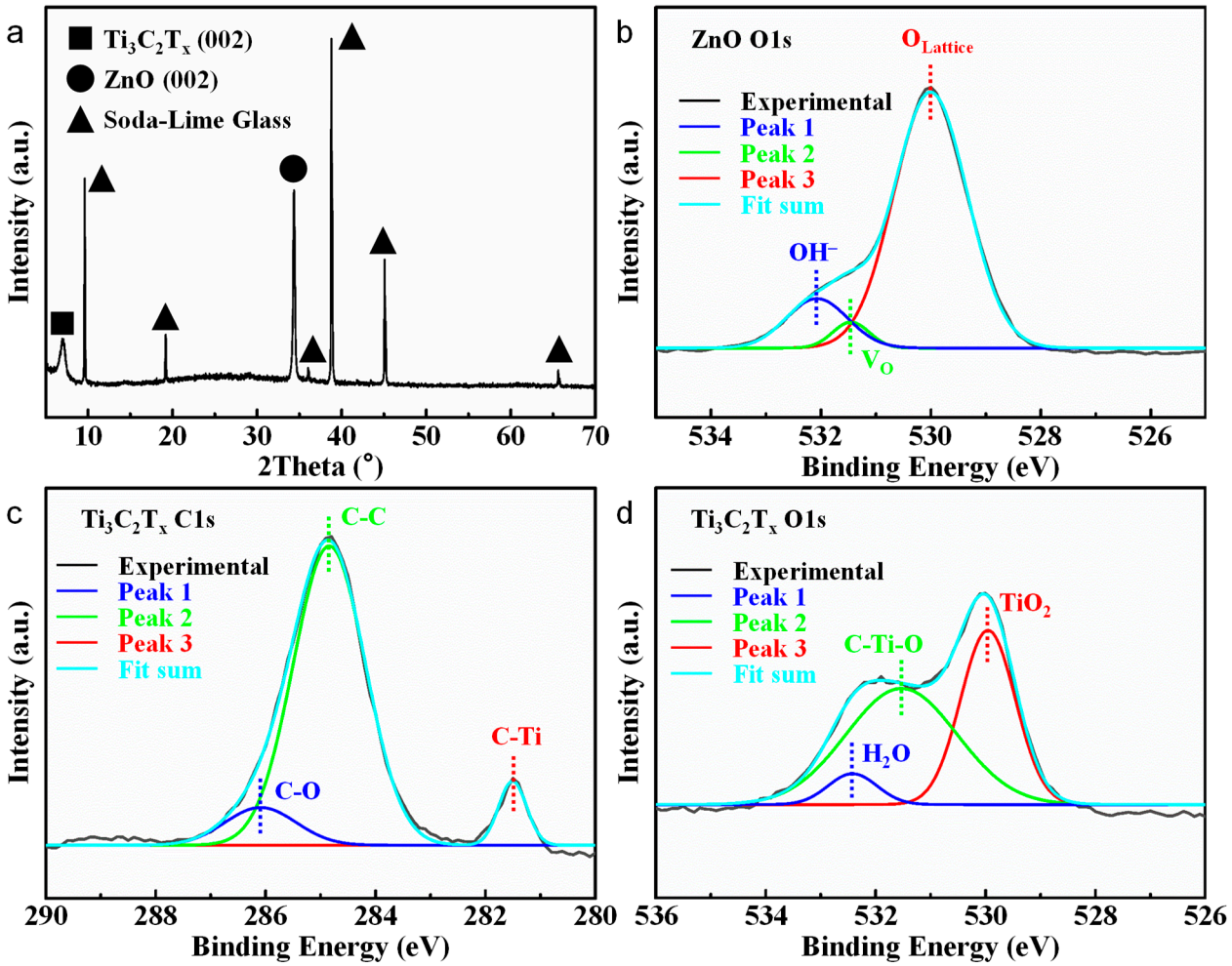

Figure S1. X-ray diffraction (XRD) and X-ray photoelectron spectroscopy (XPS) characterization results of $Ti_3C_2T_x$ MXene and ZnO.

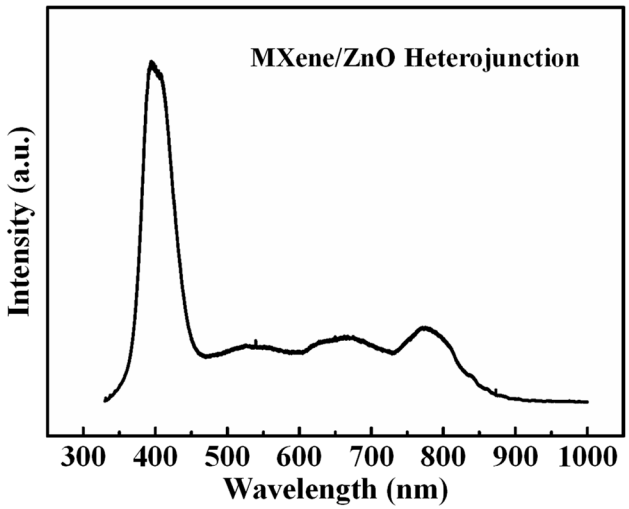

Figure S2. The photoluminescence (PL) spectrum of MXene/ZnO heterojunction.

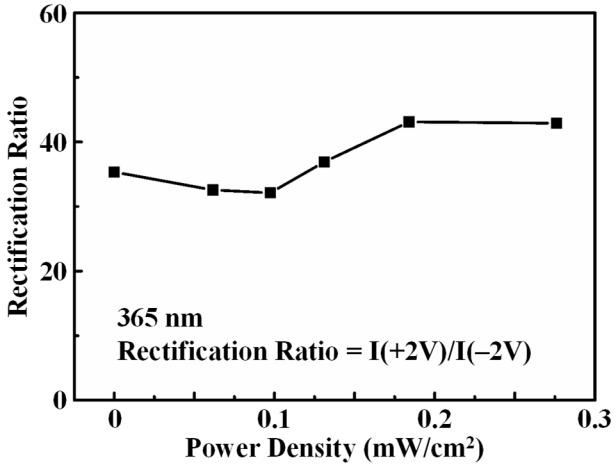

Figure S3. The rectification ratio of MXene/ZnO heterojunction under different power densities.

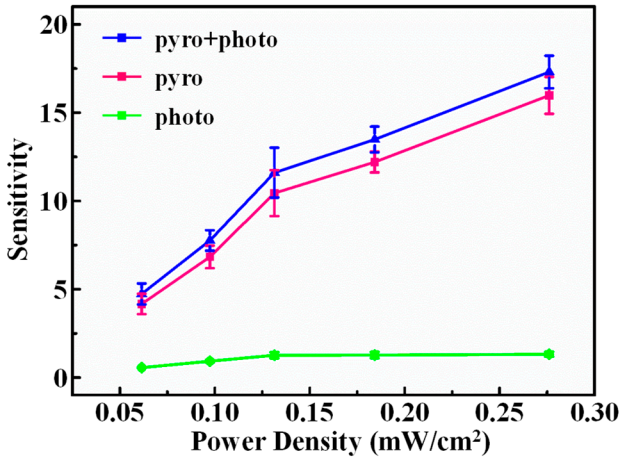

Figure S4. The sensitivity of MXene/ZnO heterojunction under different power densities.

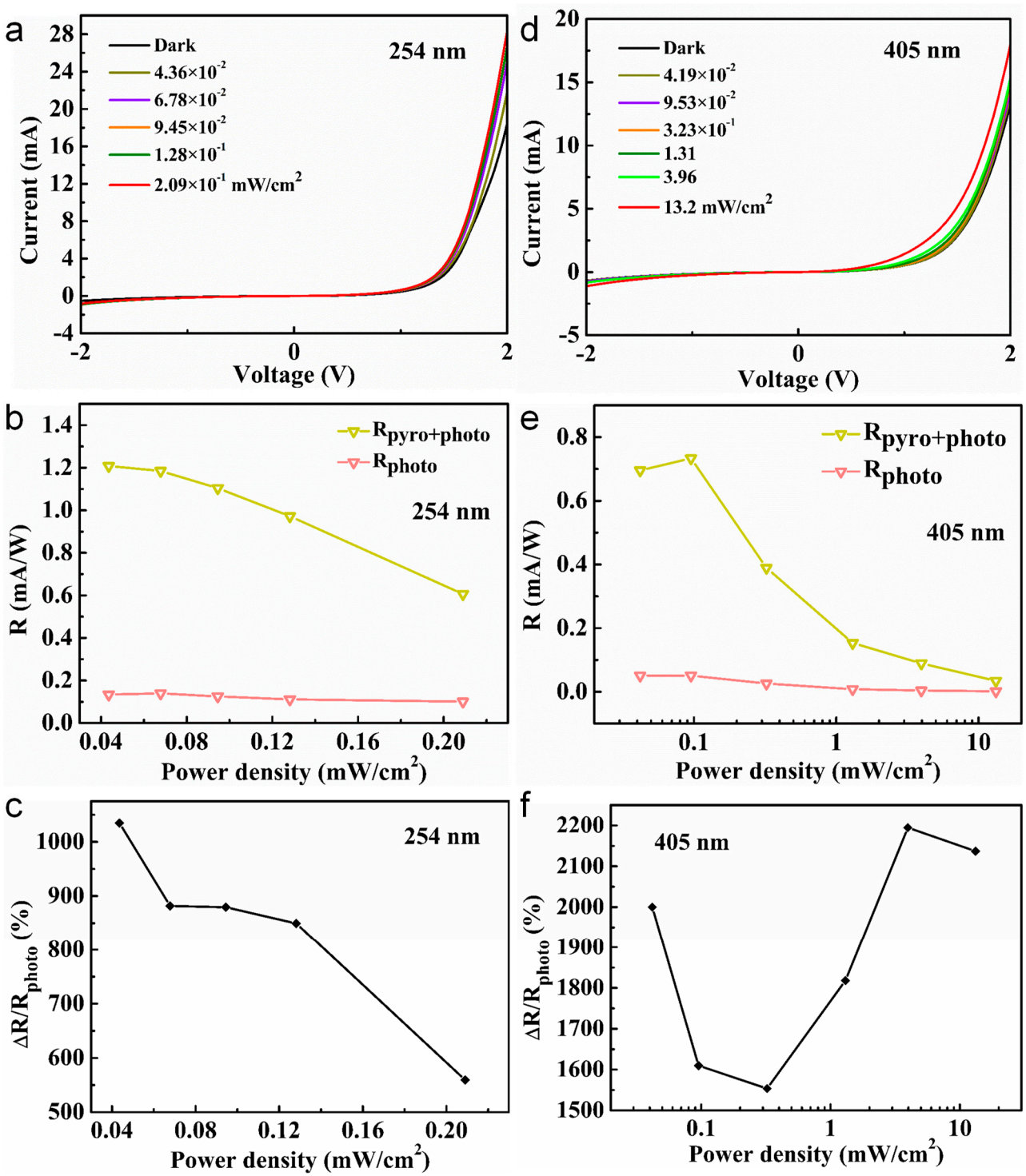

Figure S5. I–V characteristics of MXene/ZnO heterojunction under (a) 254 and (d) 405 nm illuminations. (b) Responsivity and (c) its relative variation under 254 nm illumination. (e) Responsivity and (f) its relative variation under 405 nm illumination.

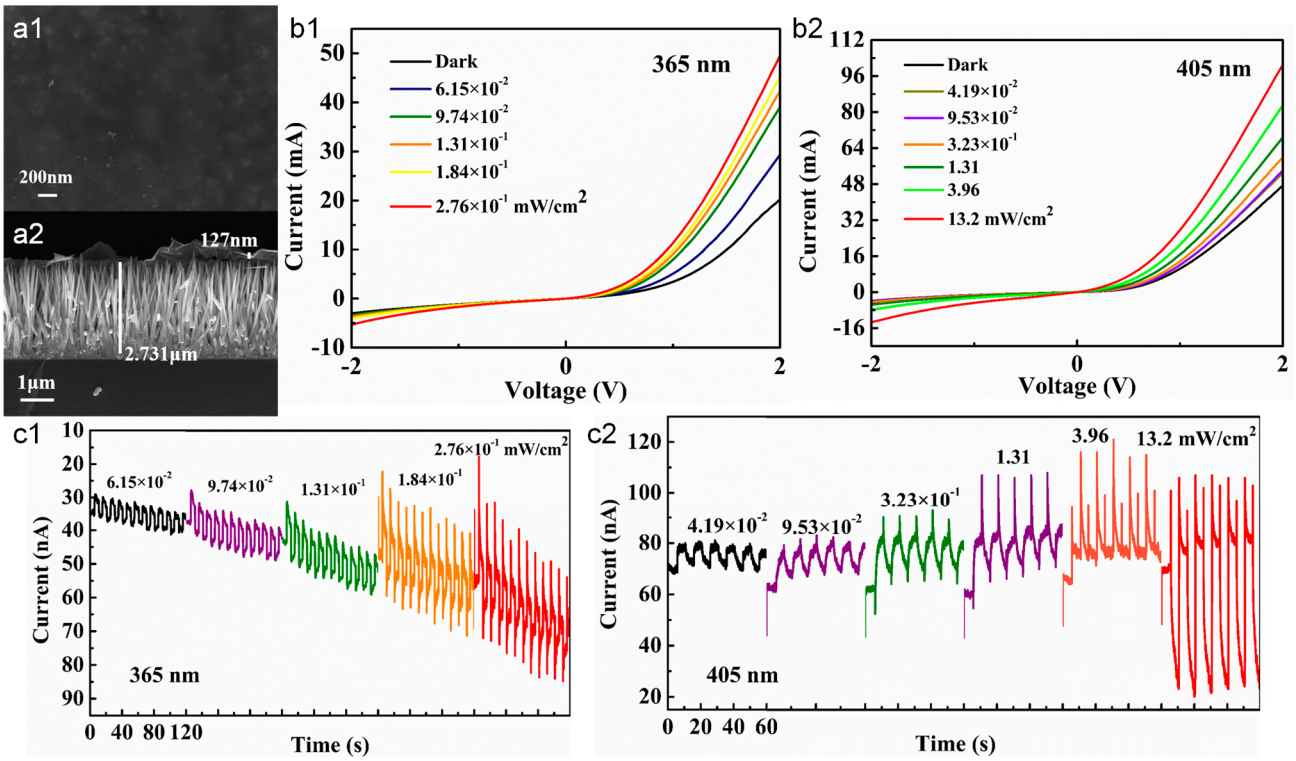

Figure S6. Characteristics of #1 sample. (a1) Top and (a2) cross–sectional view SEM images. I–V characteristics under (b1) 365 and (b2) 405 nm illuminations. Transient current under (c1) 365 and (c2) 405 nm illuminations.

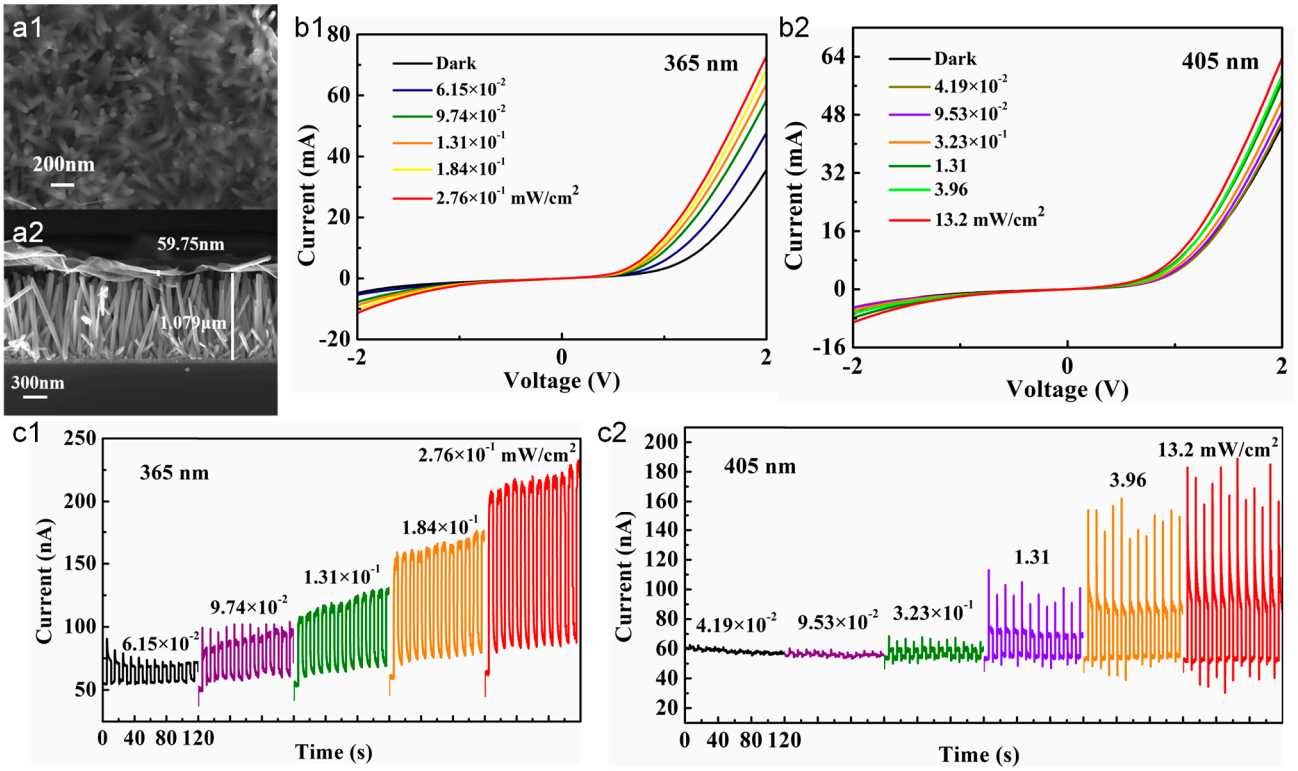

Figure S7. Characteristics of #2 sample. (a1) Top and (a2) cross–sectional view SEM images. I–V characteristics under (b1) 365 and (b2) 405 nm illuminations. Transient current under (c1) 365 and (c2) 405 nm illuminations.

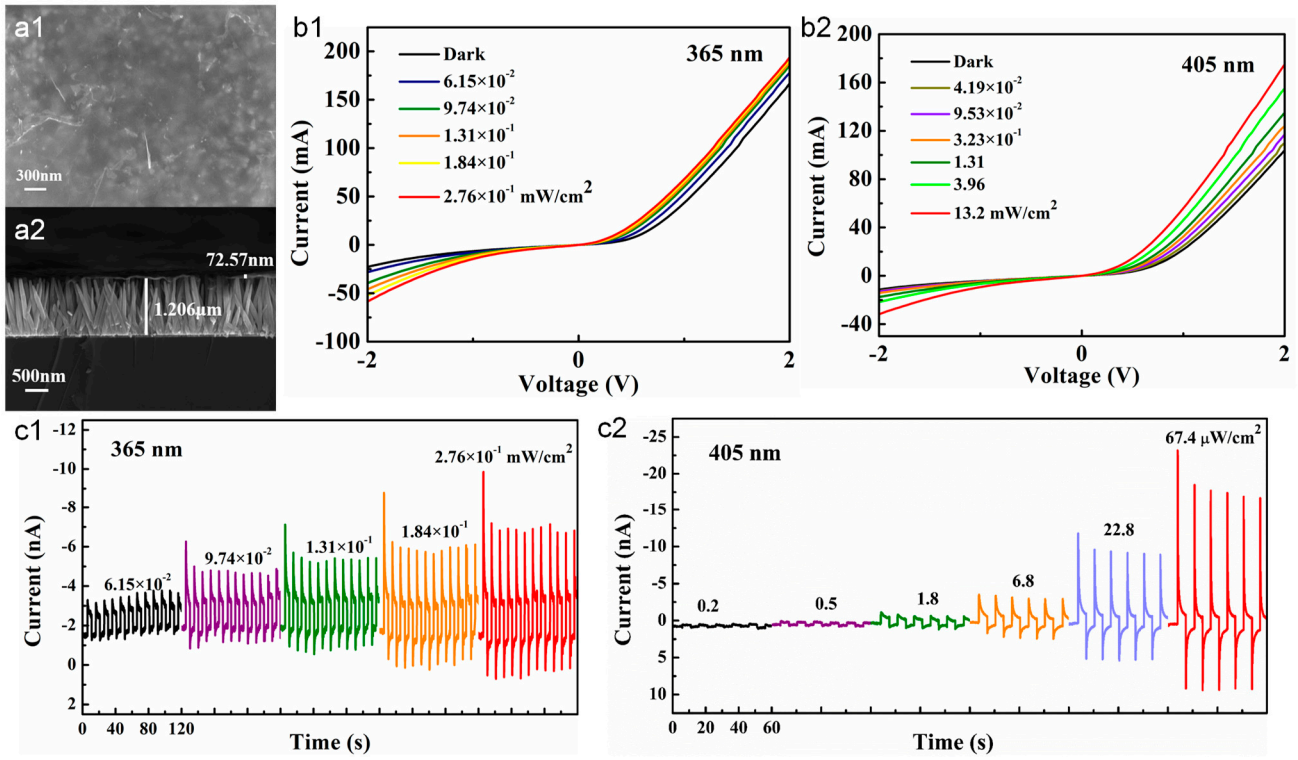

Figure S8. Characteristics of #3 sample. (a1) Top and (a2) cross–sectional view SEM images. I–V characteristics under (b1) 365 and (b2) 405 nm illuminations. Transient current under (c1) 365 and (c2) 405 nm illuminations.

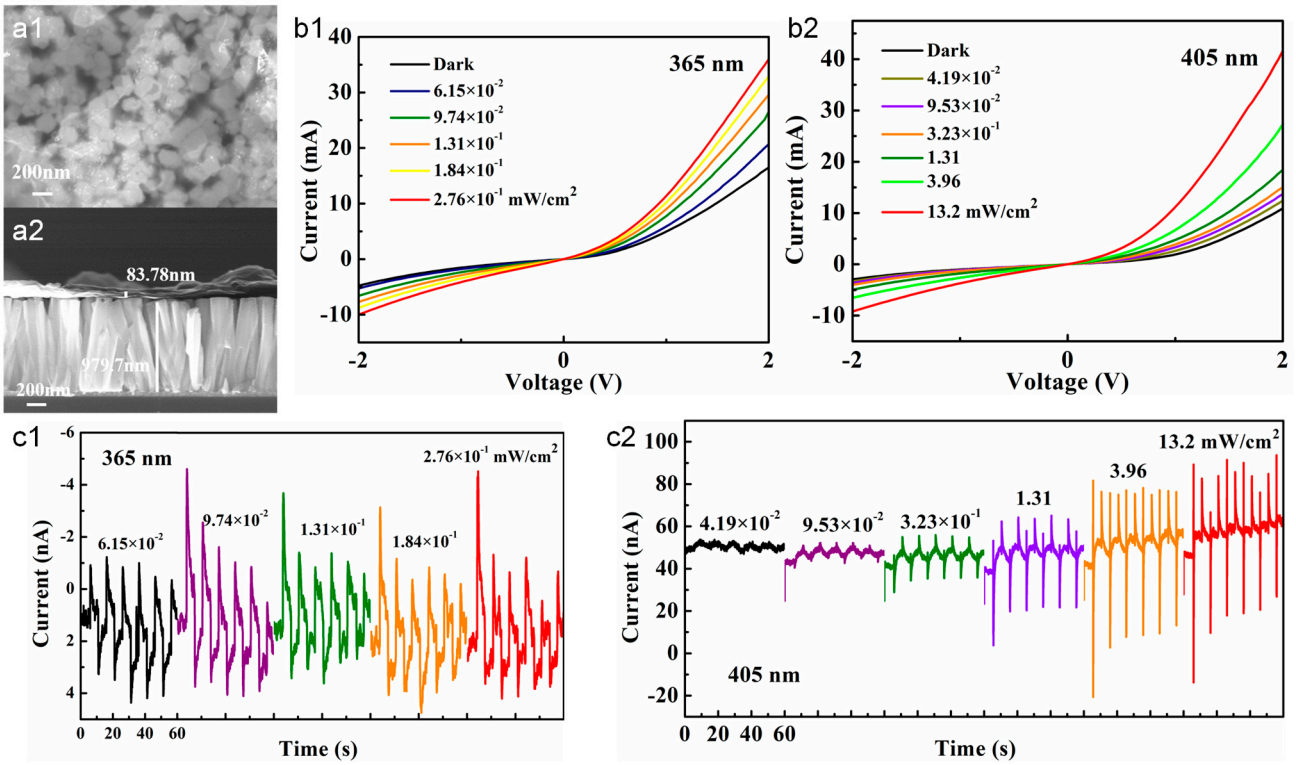

Figure S9. Characteristics of #4 sample. (a1) Top and (a2) cross–sectional view SEM images. I–V characteristics under (b1) 365 and (b2) 405 nm illuminations. Transient current under (c1) 365 and (c2) 405 nm illuminations.

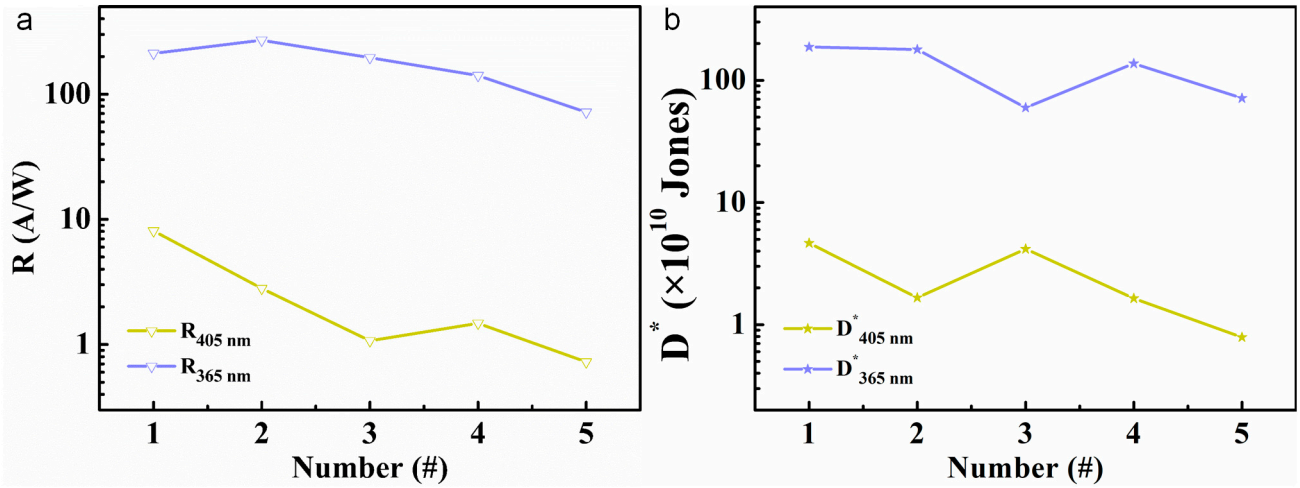

Figure S10. Comparison of (a) responsivity and (b) specific detectivity of the all five samples at +2 V bias.

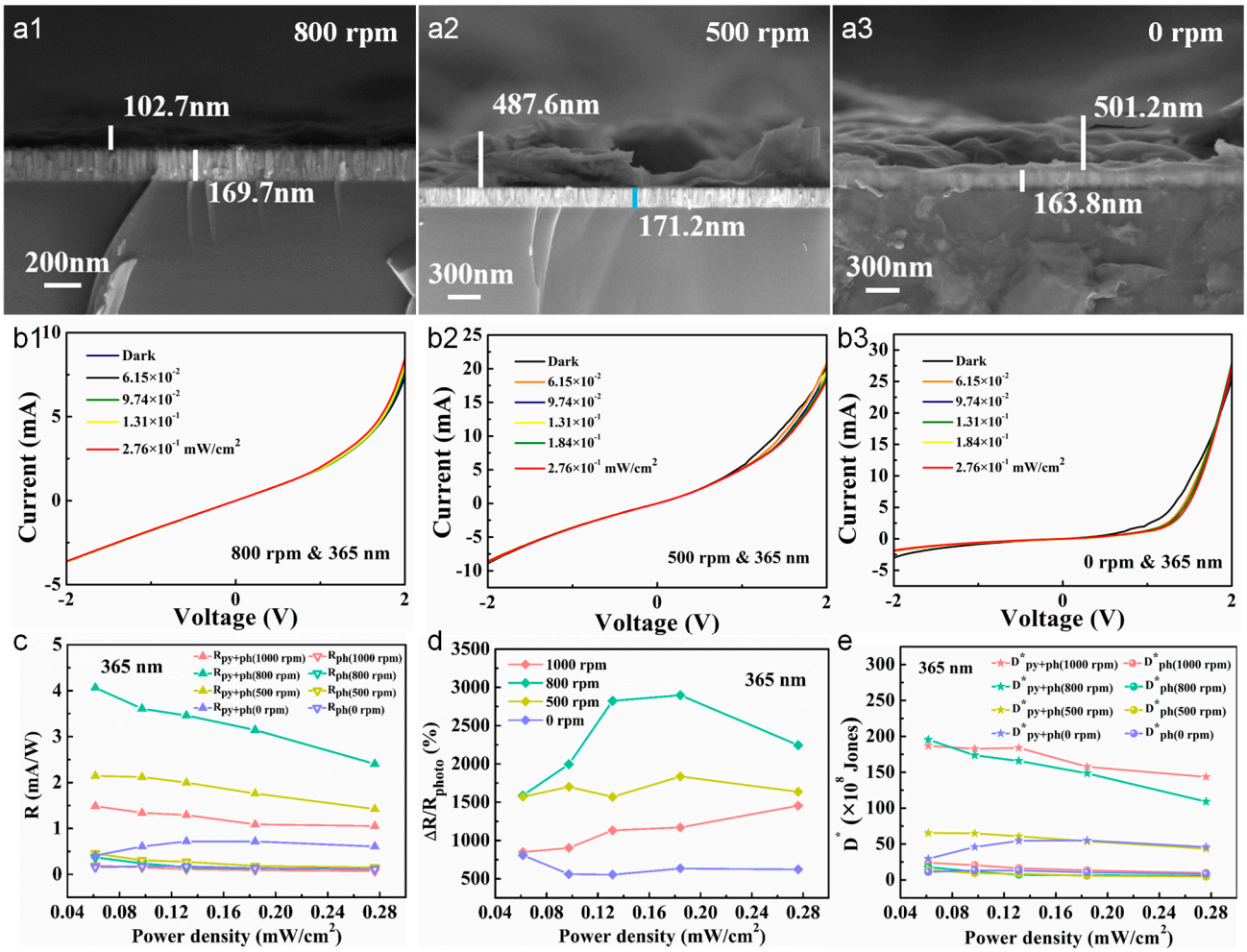

Figure S11. Influence of rotation speed of spin–coating MXene layer. Cross–sectional view SEM images of devices with (a1) 800, (a2) 500, and (a3) 0 rpm. I–V characteristics of devices with (b1) 800, (b2) 500, and (b3) 0 rpm under 365 nm illumination. The (c) responsivity, (d) relative variation of responsivity, and (e) specific detectivity of devices with different rotation speeds.

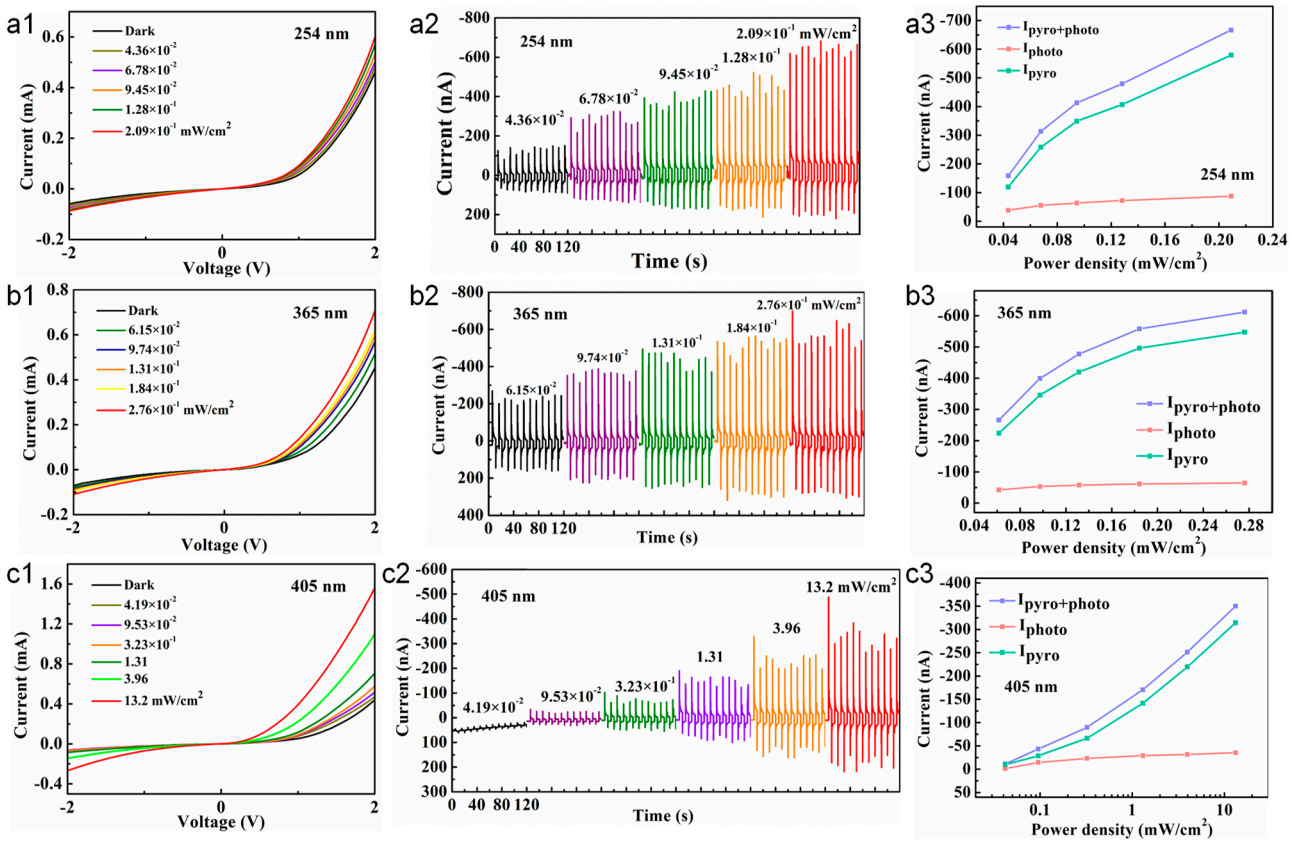

Figure S12. The fundamentals of flexible MXene/ZnO heterojunction. The (a1) I–V characteristics, (a2) transient current, and (a3) three current components of flexible device under 254 nm illumination. The (b1) I–V characteristics, (b2) transient current, and (b3) three current components of flexible device under 365 nm illumination. The (c1) I–V characteristics, (c2) transient current, and (c3) three current components of flexible device under 405 nm illumination.

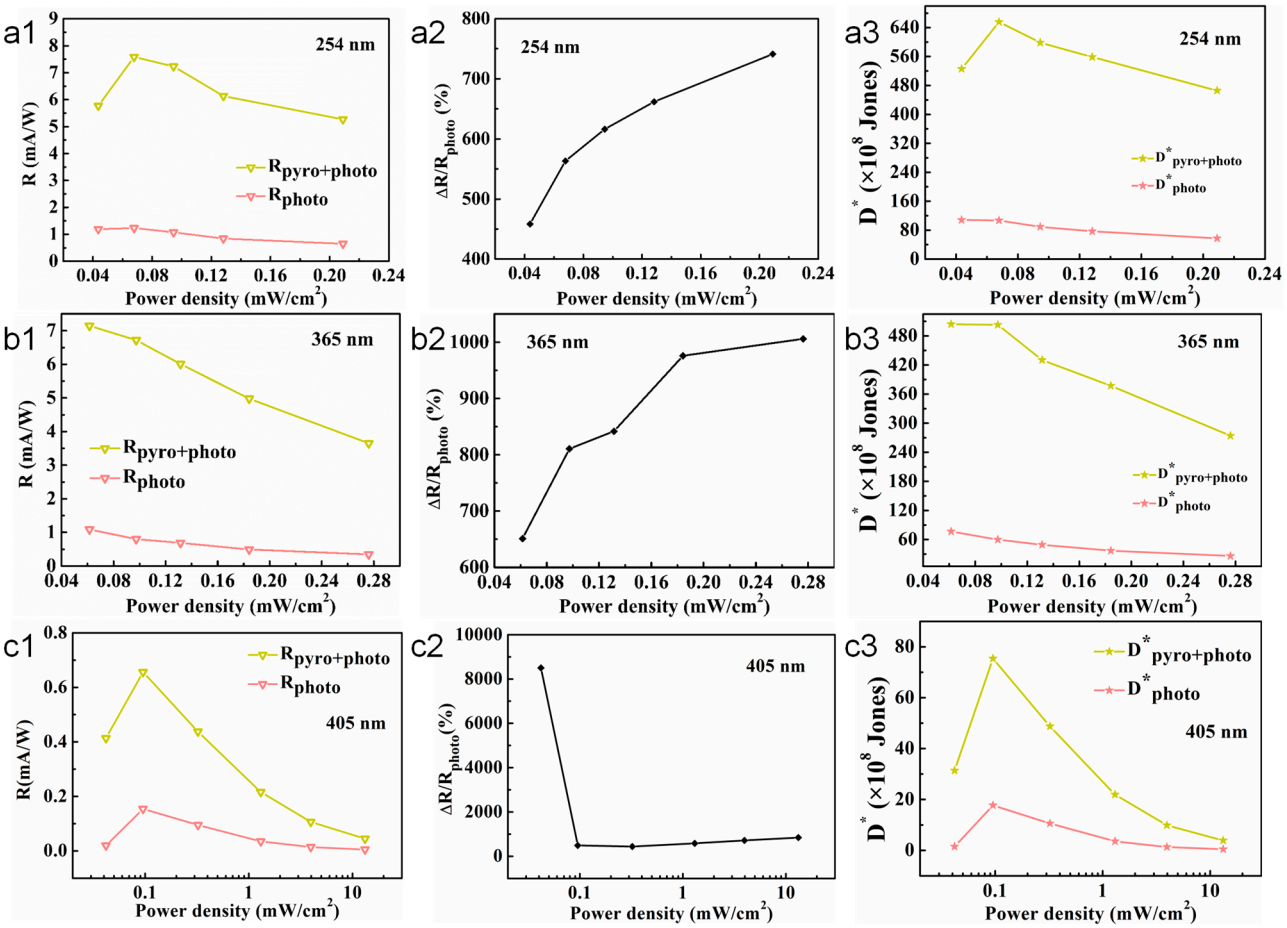

Figure S13. The performances of flexible MXene/ZnO heterojunction. The (a1) responsivity, (a2) its relative variation, and (a3) specific detectivity of flexible device under 254 nm illumination. The (b1) responsivity, (b2) its relative variation, and (b3) specific detectivity of flexible device under 365 nm illumination. The (c1) responsivity, (c2) its relative variation, and (c3) specific detectivity of flexible device under 405 nm illumination.

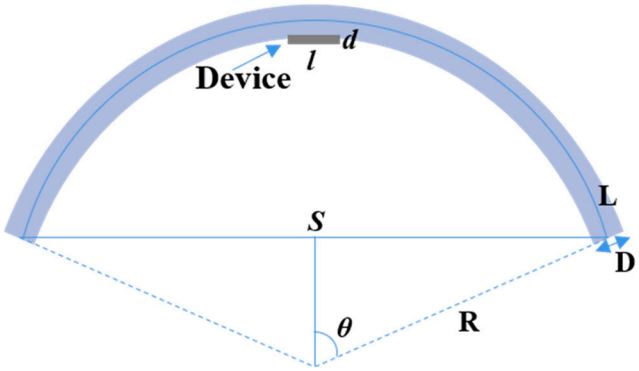

Figure S14. Schematic for calculation of applied strain to flexible MXene/ZnO heterojunction.

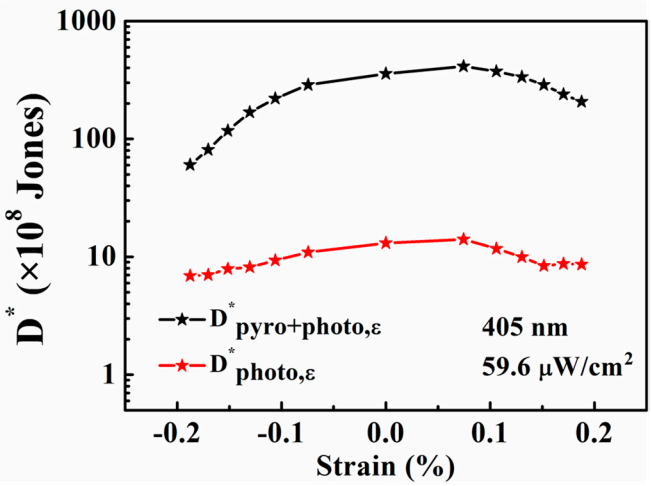

Figure S15. The specific detectivity under different strains.